JACS
JOURNAL OF THE AMERICAN CHEMICAL SOCIETY

pubs.acs.org/JACS

Article

A Dinuclear Ruthenium(II) Complex Excited by Near-Infrared Light through Two-Photon Absorption Induces Phototoxicity Deep within Hypoxic Regions of Melanoma Cancer Spheroids

Ahtasham Raza, Stuart A. Archer, Simon D. Fairbanks, Kirsty L. Smitten, Stanley W. Botchway, James A. Thomas,* Sheila MacNeil,* and John W. Haycock*

Cite This: *J. Am. Chem. Soc.* 2020, 142, 4639–4647

Read Online

ACCESS | Metrics & More | Article Recommendations | Supporting Information

ABSTRACT: The dinuclear photo-oxidizing Ru^{II} complex $[\{Ru(TAP_2)\}_2(tpphz)]^{4+}$ (TAP = 1,4,5,8- tetraazaphenanthrene, tpphz = tetrapyrido-[3,2-*a*:2′,3′-*c*:3″,2′′-*h*:2‴,3′′′-*j*]phenazine), $\mathbf{1}^{4+}$, is readily taken up by live cells localizing in mitochondria and nuclei. In this study, the two-photon absorption cross section of $\mathbf{1}^{4+}$ is quantified and its use as a two-photon absorbing phototherapeutic is reported. It was confirmed that the complex is readily photoexcited using near-infrared, NIR, and light through two-photon absorption, TPA. In 2-D cell cultures, irradiation with NIR light at low power results in precisely focused phototoxicity effects in which human melanoma cells were killed after 5 min of light exposure. Similar experiments were then carried out in human cancer spheroids that provide a realistic tumor model for the development of therapeutics and phototherapeutics. Using the characteristic emission of the complex as a probe, its uptake into 280 μm spheroids was investigated and confirmed that the spheroid takes up the complex. Notably TPA excitation results in more intense luminescence being observed throughout the depth of the spheroids, although emission intensity still drops off toward the necrotic core. As $\mathbf{1}^{4+}$ can directly photo-oxidize DNA without the mediation of singlet oxygen or other reactive oxygen species, phototoxicity within the deeper, hypoxic layers of the spheroids was also investigated. To quantify the penetration of these phototoxic effects, $\mathbf{1}^{4+}$ was photoexcited through TPA at a power of 60 mW, which was progressively focused in 10 μm steps throughout the entire *z*-axis of individual spheroids. These experiments revealed that, in irradiated spheroids treated with $\mathbf{1}^{4+}$, acute and rapid photoinduced cell death was observed throughout their depth, including the hypoxic region.

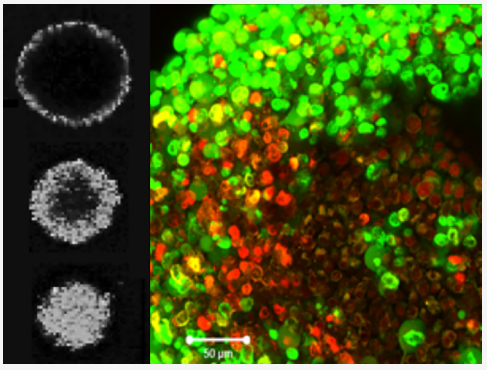

INTRODUCTION

The potential of photodynamic therapy, PDT, as a possible treatment regime was first identified over a hundred years ago,[1−3] but it only became clinically available from the 1980s.[3−8] This light driven modality requires a photosensitizer, PS, which is essentially a prodrug.[9−12] In fact, photoexcitation of the PS results in the generation of reactive molecular species and it is these species that are responsible for the therapeutic action of PDT; they are created by two common pathways,[13−15] both of which begin with the PS excited into a triple state.

In Type I reactions, the photoexcited PS participates in redox processes leading to generation of reactive oxygen species (ROS) that trigger cell death.[16] On the other hand, Type-II reactions involve the direct energy transfer from the triplet state of the PS to dioxygen thus forming highly reactive singlet oxygen ($^1O_2$), which is capable of damaging virtually all biomolecules[17−19]

PDT is still an emerging treatment technique. Consequently, although PS leads are in development, only a few systems are currently licensed.[10,20] Nevertheless, PDT offers particular potential for the treatment of skin cancers.[21−23] However, while some FDA-approved PS molecules have been tested in preclinical melanoma models demonstrating tumor regression and prolonged survival rates,[24,25] remission and reoccurrence of melanoma have also been reported.[26−28] Full clinical trials on the treatment of choroidal melanoma and metastatic skin melanoma using a clinically established sensitizer Verteporfin, and also Chorin e_6, have been reported and photoexcitation at fluences of 100 to 120 J/cm^2 produced promising therapeutic responses.[29,30] However, one of the complications with classical PDT regimes arises from hypoxia. Due to rapid growth, many tumors possess hypoxic regions, particularly at, and close to, their core.[31] Hence, incomplete treatment of tumors by PDT leading to relapse often involves these hypoxic regions where phototoxic effects are diminished.[32]

Received: October 21, 2019
Published: February 17, 2020

https://dx.doi.org/10.1021/jacs.9b11313
J. Am. Chem. Soc. 2020, 142, 4639−4647

A second potential drawback to current PDT modalities used in treating solid cancers is poor selectivity toward cancer cells. One approach to improve tumor tissue targeting over normal stroma is to activate a PS through two-photon absorption, TPA. As this requires the absorption of two photons simultaneously, activation through TPA is proportional to the square of the light source intensity and therefore only occurs at, or very close to, the focal point of the laser.[33] TPA also has an added advantage of providing a method to excite the PS in the near-infrared, NIR, therapeutic window where biological materials are most transparent, thereby providing PDT up to depths of 8 mm.[34] However, this requires a PS with an appreciable two-photon absorption cross section, TPACS (σ), and unfortunately, current commercial PS molecules have low TPACS; for example for photofrin, σ = 3 μ_B at 800 nm,[35] which results in low therapeutic effects under two photon irradiation conditions.[36,37]

An ideal PS should be amphipathic in nature, so that it can readily transverse the cellular membrane but display good water solubility, exhibit a minimum toxicity in the dark, and be photostable.[38,39] Additionally, a good TPACS would enhance treatment depths within tumors.[34,40] It is becoming apparent that these demanding criteria can be met by certain transition metal complexes.[41] The fact that complexes of d^6-metal centers can display large optical nonlinearity is well established.[42−44] At the same time, this class of complexes have been investigated as photosensitizers for PDT,[45−48] with Ru^{II} complexes attracting particular attention.[49−53] In recent work, the potential of d^6 complexes for TPA-PDT has also been delineated.[41,54−59]

In separate research, it has been found that new cancer treatments often fail clinical trials even after successful preclinical studies.[60,61] This is attributed to the fact that preclinical models usually involve either 2D cell cultures or animal models. 2D monolayer models are not capable of mimicking the complexity and heterogeneity of clinical tumors,[62,63] while *in vivo* tumor models involving nonhuman species can display discrepancies due to physiological differences between species. In response to these difficulties, humanized 3D models[64] are being developed; in particular, multicellular spheroids possess several features of *in vivo* tumors such as cell−cell interaction, hypoxia, drug penetration, response and resistance, and production/deposition of extracellular matrix.[65−69]

As part of a program to identify novel therapeutics[70−73] and phototherapeutics[74,75] based on d^6-metal complexes, we recently reported on a novel dinuclear Ru^{II} complex $[\{Ru(TAP)_2\}_2(tpphz)]^{4+}$, $\mathbf{1}^{4+}$, Figure 1 (TAP = tetraazaphenanthrene, tpphz = tetrapyridophenazine), that binds to duplex and quadruplex DNA with high affinities.[76] This complex is water-soluble, stable in serum free media, and internalized into live cells, where it predominately localizes in the nucleus and mitochondria of melanoma cells.

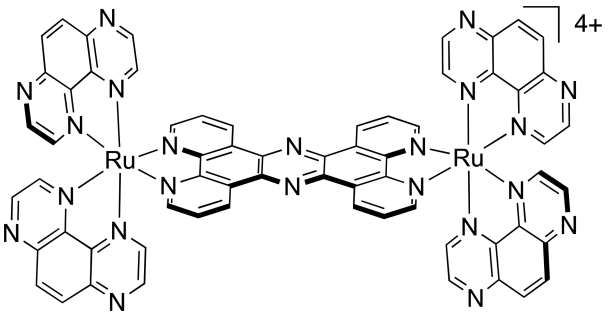

Figure 1. Structure of complex $\mathbf{1}^{4+}$.

Earlier studies have established that complexes containing electron-deficient $Ru^{II}(TAP)_2$ units possess strongly oxidizing $Ru^{II} \rightarrow TAP$ ^{3}MLCT excited states capable of *directly* photooxidizing guanine sites within DNA.[77−82] In agreement with these previous reports, detailed photophysical studies on $\mathbf{1}^{4+}$ revealed that both quadruplex and duplex DNA quench the excited state and this results in the generation of photooxidized guanine radical cation sites within the DNA. Furthermore, within 2-D melanoma cultures, we found that while $\mathbf{1}^{4+}$ is not intrinsically cytotoxic, it is activated by light; for example, irradiation with low fluences of LED light at 405 nm rapidly induced apoptosis in human C8161 melanoma cells, effectively resulting in zero cell viability.[76]

Complex $\mathbf{1}^{4+}$ was developed as a photoredox active analogue of the metal complex $[\{Ru(phen)_2\}_2(tpphz)]^{4+}$ (phen = phenanthroline) which has been successfully used as a live cell TPA optical imaging probe.[83] Given that $\mathbf{1}^{4+}$ is capable of directly damaging biomolecules without the mediation of $^1O_2$ or other ROS, that it localizes in both nuclei and mitochondria, which are specific targets for PDT,[9,48,84,85] and the fact that it is related to a system with an appreciable TPACS, we reasoned that this complex could be developed as a PS to initiate PDT effects at tissue depths where hypoxia occurs and normal PDT regimes are ineffective.

Herein, we report that $\mathbf{1}^{4+}$ functions well as a PS in TPA conditions and as a consequence the complex facilitates high spatial resolution phototoxicity within an engineered spheroid model of the highly invasive and spontaneously metastatic, recalcitrant human skin cancer, C8161 melanoma.[28] Furthermore, as the complex is luminescent, and its emission properties are compatible with optical microscopy, we can directly track the penetration of this theranostic deep into this tumor model.

Virtually no studies on metal complex photosensitizers and spheroids have been reported. The Chao group recently reported on Ru^{II}-complexes for TPA-PDT in HeLa-based spheroids, but their work involved PSs that function through a classic oxygen-dependent Type II mechanism, whereas the photodamaging mechanism of $\mathbf{1}^{4+}$ is independent of ROS and $^1O_2$. As the employed spheroid model contains healthy, hypoxic, and necrotic layers, these studies have afforded insights into the effectiveness of the new PS in a realistic tumor environment containing both quiescent and proliferative areas. Consequently, the use of this preclinical human tumor model has provided detailed information on PS penetration, light penetration, responsiveness dosage, and resistance area that could only previously be obtained by animal studies in immune compromised animals or clinical trials.

RESULTS AND DISCUSSION

We first investigated the TPACS of $\mathbf{1}^{4+}$ through an adaption of a previously reported method[86] (see Materials and Methods for details). This led to an estimate maximum TPACS of σ = 90 GM, which is up to double that of commercial sensitizers that have been investigated for TPA-PDT.[87,88]

We then went on to investigate emission within the melanoma cells using TPA conditions, which revealed optimal emission outputs from the internalized complex on excitation at 850−900 nm (Figure 2), confirming that it could be

https://dx.doi.org/10.1021/jacs.9b11313
J. Am. Chem. Soc. 2020, 142, 4639−4647

photoexcited in these conditions using NIR light, well within the therapeutic window.

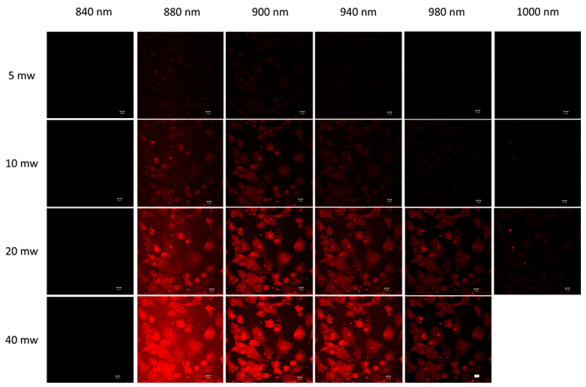

Figure 2. Emission from $\mathbf{1}^{4+}$ internalized within human melanoma cells following a TPA laser excitation over a wavelength range of 840–1000 nm and power range of 5–40 mW (scale bar = 10 μm).

The TPA-PDT potential of $\mathbf{1}^{4+}$ was next investigated in a monolayer of human C8161 melanoma cells incubated with 100 μM of $\mathbf{1}^{4+}$ for 24 h to ensure complete internalization. A discrete 250 × 250 pixel region of interest (ROI) was marked in a 512 × 512 pixel frame and irradiated with 900 nm laser light (10 and 20 mW). The ratio of live and dead cells were determined before and after the irradiation (every 5 min) using Syto-9 (cell indicator) and PI as live and dead cell markers respectively; see Supporting Information (SI) and Figure 3. This experiment revealed that, at 10 mW, 30 min exposure time was required before any phototoxicity was observed in irradiated cells within the ROI (see SI), while, at 20 mW, the entire ROI showed complete melanoma death after 5 min of exposure (Figure 3). The photoxic effect was observed in

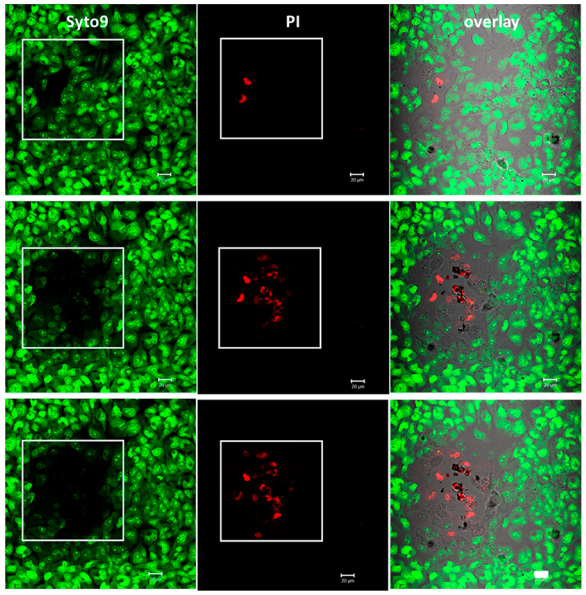

Figure 3. Two-photon phototoxicity of $\mathbf{1}^{4+}$ in human melanoma cells treated with $\mathbf{1}^{4+}$ (100 μM) after irradiation within the marked white square at 900 nm. Live/dead cells imaged with (left column) Syto-9 (2 μM), (middle column) Propidium iodide (500 nM), and (right column) combined image. Recorded at 0 min (top row), 5 min (middle row), and 10 min (bottom row) (scale bar = 20 μm).

melanoma cells only in the presence of Ru–Ru TAP, and not in response to two-photon-laser irradiation alone under identical conditions (see SI).

Apoptosis and necrosis are cell death defined responses to a stimulus. , Cell death In response to Ru(II) plus light activation was studied using Annexin V and propidium iodide (PI). Furthermore, morphology changes of cells (by H and E) and cytoskeleton filament (F-actin) structures were also studied. Both apoptosis and necrosis were noticed within the cell population after PDT treatment. Cell size was decreased, and actin filaments were damaged, with shrinkage in nuclear size and cell blebbing, suggesting necrosis as the prominent cause of death (see SI).

We have previously established that C8161 human melanoma spheroids cultured for 10 days (at an initial seeding density of 12 000 cells) have an outer proliferative area of approximately 100 μm in depth over a second layer of hypoxic cells that is also approximately 100 μm thick. The remaining central volume of the spheroid forms a necrotic core.[89] These features provide an opportunity to study the PDT effect of $\mathbf{1}^{4+}$ in a live multicellular 3-D tumor model that has both proliferative and hypoxic regions and thus assess the therapeutic effectiveness of this PS in low oxygen conditions. In these experiments we first explored photoexcitation of $\mathbf{1}^{4+}$ at various depths within tumor spheroids using conventional one-photon excitation at 458 nm and two-photon excitation (λex = 900 nm). Although luminescence was observed throughout the 280 × 280 μm spheroid, indicating that the complex penetrates deep into the spheroids, emission intensity using either excitation regime noticeably decreases toward their center.

This decrease in signal is probably caused by a combination of two effects: (1) there is a concentration gradient for the complex that diminishes with spheroid depth and/or (2) light penetration into the center of the spheroid is too low to photoexcite $\mathbf{1}^{4+}$. Nevertheless, a comparison of emission produced by 1PA and TPA at analogous laser powers reveals that, as expected, NIR excitation results in higher intensity emission at depths (Figure 4). These results reveal that photoexcitation of the complex to a depth of ~240 ± 20 μm in the z-axis can be readily accomplished.

Consequently, the therapeutically effective dose of $\mathbf{1}^{4+}$ in melanoma spheroids using a two-photon excitation regime was evaluated. In particular, the effect of laser power on exposure to $\mathbf{1}^{4+}$ at a concentration of 100 μM was quantified. Initially excitation through laser irradiation at 900 nm was focused on the spheroid outer proliferative layer at fluxes of 20, 40, and 60

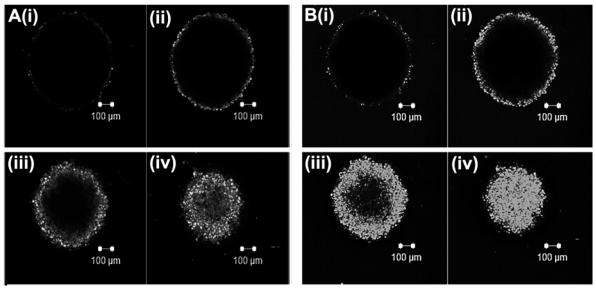

Figure 4. Comparing the luminescence of $\mathbf{1}^{4+}$ in a 280 μm × 280 μm C8161 human melanoma spheroids following: (A) one-photon excitation (458 nm) and (B) two-photon excitation (900 nm) at a power of 10 mW. Intensities measured at z-stack depths of (i) 0 μm, (ii) 60 μm, (iii) 180 μm, and (iv) 240 μm (scale bar = 100 μm).

https://dx.doi.org/10.1021/jacs.9b11313
J. Am. Chem. Soc. 2020, 142, 4639–4647

mW, respectively. Live and dead cells were quantified before irradiation and then at every 15 min using Syto-9 and PI, respectively (Figure 5).

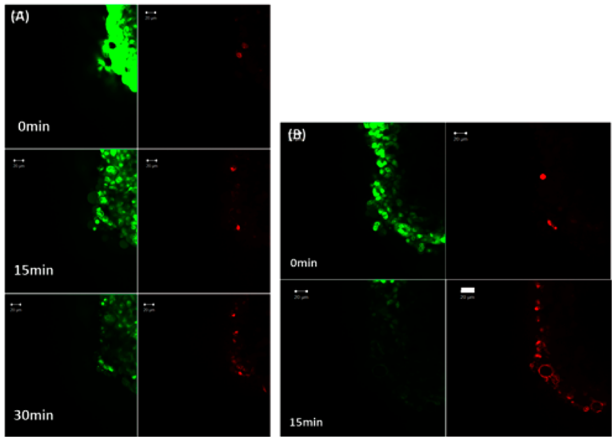

Figure 5. Two-photon PDT in a human melanoma spheroid outer proliferative area region with a 900 nm laser and powers of (A) 40 and (B) 60 mW after treatment with 100 μM of $\mathbf{1}^{4+}$ for 24 h. Left: live cells imaged with Syto-9. Right: dead cells imaged with PI. In spheroids untreated with $\mathbf{1}^{4+}$, illumination at either power produced no increase in cell death (scale bar = 20 μm).

These experiments showed that although no cell death occurred at 20 mW flux, at 40 mW the proliferative region of the spheroid was eradicated after 30 to 45 min of exposure (Figure 5a) and irradiation at 60 mW produced the same effect after only 15 min of light exposure (Figure 5b). Negative control experiments confirmed that spheroids untreated with $\mathbf{1}^{4+}$ showed no increase in cell death on laser irradiation confirming that the photosensitization of the spheroids requires $\mathbf{1}^{4+}$. The differences in the irradiance dose for monolayer cultures compared to melanoma spheroids illustrate how the use of 3D spheroids provides an improved preclinical model for lead development.

Next we investigated the depth of the phototherapeutic effect of $\mathbf{1}^{4+}$ within the spheroid. Depending on cancer stage, human melanoma tissue thickness can vary; consequently, PDT treatment will be optimized when a PS penetrates and activates at specific depths. To investigate this possibility, a point on the surface of the spheroid was chosen and then laser irradiation at a power of 40 mW or 60 mW was focused at *z*-axis depths that progressively increased in 10 μm steps (Figure 6 and SI). Again, the ratio of live and dead cells in this z-stack was determined before irradiation and every 15 min thereafter using Syto-9 and PI. At 40 mW laser power, minimal evidence of phototoxicity at depth was observed after 30 to 45 min, but at 60 mW the continuous z-stack scan revealed cell death within 15 to 30 min. Significantly, although the phototoxic effect was at its greatest between 0 to 80 μm, cell death was observed throughout the entire *z*-axis depth of the spheroid (Figure 6C), showing that cell killing occurred in the hypoxic regions of the spheroid. A similar analysis of light-induced cell death across the entire 300 × 300 μm^2 $x-y$ plane at 60 mW revealed that phototoxic effects can be seen through the entire *xy* plan, even at depth.

CONCLUSION

Lamp light sources commonly used for conventional PDT are in an energy range of 60 to 200 J/cm^2 (commonly with flux rates of 150 mW/cm^2).[90] Although a high flux rate does reduce treatment time, it often causes hyperthermia and a reduced photodynamic effect due to oxygen depletion.[91−94] Furthermore, although lamp sources are suitable for treatment of large skin area, they cannot be focused on small specific lesions. In contrast, as laser excitation volumes of a few femtoliters can be attained by two-photon excitation, high spatial selectivities can be obtained providing the potential to selectively treat melanoma without deleterious effects on surrounding tissue. Furthermore, excitation of a PS through TPA at 900 nm avoids a known mechanism of PDT resistance in melanoma; the abundance of melanin in such pigmented tumors means that light that should excite the PS is instead absorbed by melanin.[26,95,96] This "filter" effect means that transmittance

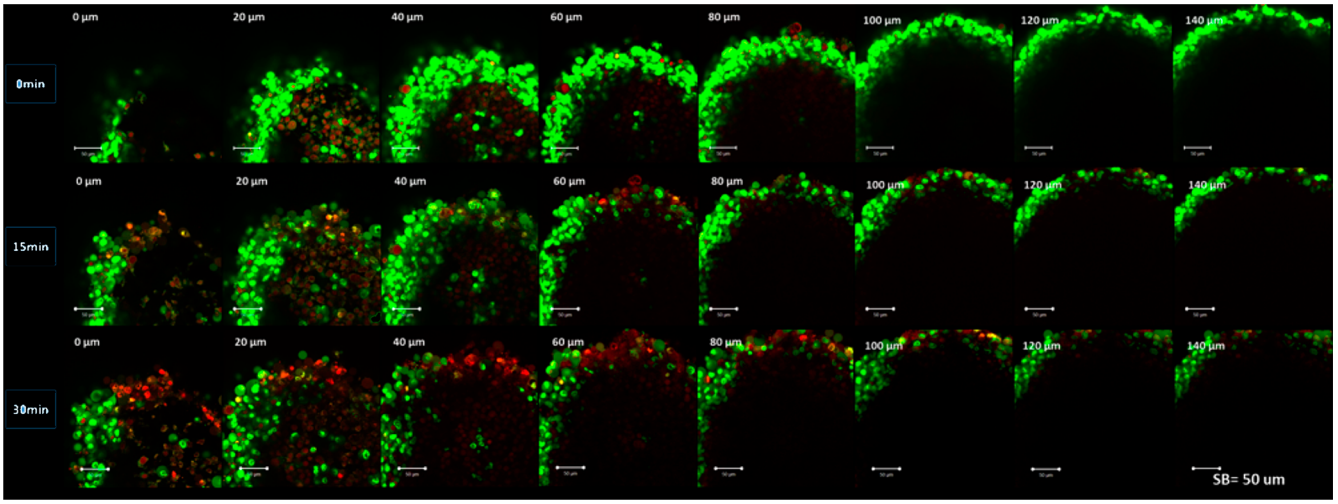

Figure 6. TPA-PDT on human melanoma spheroids cultured for 10 days. Spheroids were then allowed to settle on a 35 mm plate overnight and incubated with $\mathbf{1}^{4+}$ (100uM), propidium iodide (500 nM), and Syto-9 (2 μM) in SFM for 24 h. Spheroids were irradiated with a 900 nm laser (power = 60 mW) using a continuous z-stack scan (10 μM apart) for 30 min. This was followed by a live and dead cell scan through the whole spheroid. Live/dead scan at specific depths before treatment revealing hypoxic/necrotic central region (before treatment, top). Analogous live/dead scans 15 min (middle) and 30 min (bottom) after irradiance (scale bar = 50 μm).

https://dx.doi.org/10.1021/jacs.9b11313
J. Am. Chem. Soc. 2020, 142, 4639−4647

through melanoma only occurs at wavelength above 700 nm.[27,97]

In summary, given that NIR photoexcitation of 1^{4+} through TPA allows phototoxic effects to be delivered with high precision into the depths of a therapeutically relevant and realistic tumor model to induce cell death even in hypoxic conditions, this complex is a highly promising lead for focused PDT regimes. By exploiting structural "ground rules" used to optimize TPACS,[33,57] new derivatives of this lead complex with enhanced two-photon excitation properties are currently being targeted. Ongoing work exploring the use of this PS in more sophisticated preclinical models will form the basis of our future reports.

MATERIAL AND METHOD

Complex 1^{4+} was synthesized through a reported method.[76]

Estimate of Two-Photon Absorption Cross section. The value of the two-photon absorption cross section was calculated according to the following modified equation presented by Rebane and co-workers[86]

$$\sigma_s = (c_r/c_s)*(I_s/I_r)*(FI\,\lambda_s/FI\,\lambda_r)*\left(\sum I_r/\sum FI_s\right) *(\Phi_r\Phi_s)*\sigma_r \quad (1)$$

where σ is the two-photon absorption cross section, I is two-photon intensity, Fl (one-photon emission intensities at l), $\sum$FI is the integrated one-photon intensity, c is the molar concentration (r,s are reference and sample), and φ is the differential emission quantum yield in the spectral range: 608−620 nm. The differential emission quantum yield of Rhodamine B was taken as 0.5. The value σ_r for Rhodamine B in MeOH was taken as 180 GM at 850 nm and 13 GM at 900 nm.[86] The differential quantum yield φ was obtained on a Jobin-Yvon Fluoromax 4 fluorimeter under one-photon excitation. However, in order to achieve good spectral agreement for the reference under one- and two-photon excitation, a lower solution concentration was required for single-photon measurements. The emission maxima and QY of Rhodamine B in MeOH are known to vary with sample concentration. Therefore, the two-photon absorption cross section values were calculated using Rhodamine B QY which corresponds to the solution used (i) for two-photon measurements (QY = 0.4[5]) and (ii) for single-photon measurements (QY= 0.65[5]). The difference between the two calculations is approximately 50%. Thus, a range of ∼7 (@ 900 nm) to 90 (@850 nm) GM was estimated. These errors are due to several factors including the small values and uncertainties of rhodamine B two-photon cross section at 900 nm (which is 13 GM).

Human Melanoma Cell Culture. The C8161 human melanoma cell line was isolated from an abdominal wall metastasis from a recurrent malignant melanoma menopausal woman (and a gift from Professor F. Meyskens UC Irvine (USA) via Dr. M. Edwards (University Glasgow, UK)). C8161 melanoma cells were grown in melanoma culture medium consisting of EMEM media (Sigma-Aldrich) supplemented with FCS (10% v/v), L-glutamine (2 μM), Pencillin (100 U/mL), streptomycin (100 μg/mL), and Amphotericin (0.625 μg/mL).

Intracellular Localization in Human Melanoma Cell Line. C8161 melanoma cells were grown in 6-well plates for 24 h at 37 °C. The cells were washed with SFM and incubated with 100 μM RuRuTAP for 1, 6, 12, and 24 h in the dark at 37 °C. For mitochondria, nucleus, and lysosome colocalization, the cells were further incubated with Mitotracker (200 nM), Lysotracker (100 nM), and DAPI (300 nM, for 15 min) for 1 h. Cells were washed with SFM and fixed with formaldehyde (3.7%, 15 min). Cell imaging was performed after cells were washed with PBS (thrice, 5 min).

Photocytotoxicity Using 405 ± 20 nm Lamp in Human Melanoma Cell Line. C8161 melanoma cells were grown in 24-well plates (1×10^5 cells/well) for 24 h at 37 °C. Cells were then incubated with increasing concentrations of 1^{4+} (0, 10, 50, 10, 200 μM) for another 24 h in the dark at 37 °C. The compound was then removed, and cells were washed with SFM and replenished with SFM. The plates were then irradiated (6.01 J (1 h), 12.04 J (2 h), and 18.03 J (3 h), using a ThorLabs LED (M405LP1) with an emission of 405 nm (±20 nm) and power output of 1500 mA. The LED was fixed on a metal stand (20 cm from base). After the irradiance, the SFM was replaced with serum containing medium and cells were incubated for 18 h. Alamar blue (Resazurin Na salt, 100 μM for 4 h in SFM) was used to measure the cell viability.

Apoptosis Assay (Annexin V and PI Staining). Apoptosis and/or necrosis cell death are two defined pathways. To distinguish the cellular death pathway after the stimuli (1^{4+} at 100 μM for 24 h with and without 1-h 405 nm light irradiance), Annexin V Fluor-488 and PI (Invitrogen, V13241) were utilized. Briefly, C8161 melanoma cells were seeded on a 6-well plate for 24 h and then treated with or without 1^{4+} (100 μM for 24 h in SFM), and the plates were then irradiated or kept in the dark for 1 h using a lamp (405 nm). Afterward, the plates were incubated with Annexin V and PI (10 μg/mL and 500 nM, respectively) for 30 min and washed with annexin binding buffer (thrice, 5 min). Cells were then fixed (formaldehyde 3.7%, 15 min) and washed with PBS (×3, 5 min), followed by counterstaining with DAPI and imaging under a Zeiss LSM510 confocal microscope using an Achroplan water dipping objective (40×, NA 0.75, WD 2.1).

Two-Photon Absorption Cross section Imaging. C8161 melanoma cells were incubated with 1^{4+} at 100 μM concentration (in SFM) for 24 h. Cells were then washed with PBS (×3) and fixed with 3.7% formaldehyde (15 min). Luminescence images of 1^{4+} within were taken between 800 to 1000 nm by confocal microscopy (attached to Ti-sapphire Chameleon FD900 laser) with an Achroplan objective (40×/0.75 W, Scan speed of 6 r). The average optical power of each wavelength studied was altered to four different powers (5, 10, 20, and 40 mW). The resultant emission images were collected at λ_{em} = 630−700 nm from varied excitation wavelengths and four different power settings. To attain an ideal cross section value, the emission profile was used to calculate corrected fluorescence emission intensity using ImageJ.

Uptake and Distribution 1^{4+} in 3D Melanoma Spheroids. Melanoma spheroids were formed using C8161 human melanoma cell lines using a liquid overly method as described previously.[89] Briefly, an initial cell seeding density of 12K were cultured in a 96-well plate coated with agarose gel (1.5% w/v) for 10 days (at 37°C and 5% CO_2).

To measure 1^{4+} distribution through the melanoma spheroids (MCTS), spheroids after 10 days of culture were removed and transferred to 35 mm glass bottomed dishes (3−4 MCTS in each dish) and allowed to incubate at 37 °C (5% (v/v) CO_2) overnight to settle. 1^{4+} at 100 μM concentration was incubated for a period of 24 h. Before analysis, MCTS were washed with SFM (×3) and kept immersed in SFM during data collection upon two-photon excitation (λ_{ex} = 900 nm, λ_{em} = 630−700 nm). A Zeiss LSM510 META upright confocal microscope, connected to a two-photon class 4 tunable Ti-sapphire Chameleon laser (FD900, Coherent) and an Achroplan water dipping 40× objective lens (WD 2.1 mm, NA 0.75), was used to image the 1^{4+} emission through the full depth of the spheroid. Optical slices were taken at 10 μm apart in each sample to create a 3D (Z-stack) construct image. The depth of penetration was between first and last fluorescence optical slice. Frame size (512 × 512) scan direction (single), scan speed (6), laser power (20 mW), and detector gain (874) were kept constant for all repeats.

Two-Photon Photocytotoxicity in Melanoma Cells. Human melanoma C8161 cells were seeded on a 35 mm dish plate (5×10^5 cells/well). After incubation for 24 h, the cells were treated with or without 1^{4+} at 100 μM concentration (in SFM) for 24 h. The cells were washed with serum-free culture medium (×3) and replenished with live and dead medium (propidium iodide (PI at 500 nM) and Syto-9 (2 μM) in SFM) for 15 min and through the length of time of experiment. The monolayer of cells was imaged for live cells (Syto-9, λ_{ex} = 488 nm (Ar-ion), λ_{em} = 500−550 nm) and dead cells (PI, λ_{ex} = 543 nm, λ_{em} = 565−615 nm). Live and dead cells images were taken

https://dx.doi.org/10.1021/jacs.9b11313
J. Am. Chem. Soc. 2020, 142, 4639−4647

from the same area (512 × 512 pixel) after every 5 min of irradiation at 900 nm at 10 and 20 mW (scan speed = 6) on a marked region of interest (250 × 250 pixel). Irradiation was carried using a Ti:sapphire laser (Cameleon, Coherent) connected to a Zeiss confocal microscope (LSM510) using an Achroplan water dipping objective (40×, NA 0.75, WD 2.1).

Two-Photon Photocytotoxicity in Melanoma Spheroids. Photocytotoxicity in 3D melanoma spheroids was also imaged using the same method discussed above. However, the laser power for irradiation was increased to 20, 40, and 60 mW. After the ideal cytotoxic response at 60 mW at a single optical slice was attained, spheroids were irradiated with a 60 mW 900 nm two-photon laser using a continuous z-stack (10 μM optical slice apart) scan (scan speed = 6); the irradiance dose though the whole thickness of the spheroid was followed by live and dead cell scan through the whole spheroid.

■ ASSOCIATED CONTENT

Supporting Information

The Supporting Information is available free of charge at https://pubs.acs.org/doi/10.1021/jacs.9b11313.

Intracellular localization and uptake in melanoma cells; apoptosis and necrosis caused by PDT on melanoma; Two-Photon phototoxicity without $\mathbf{1}^{4+}$; Imaging showing TPA-PDT of whole thickness of melanoma spheroid (PDF)

■ AUTHOR INFORMATION

Corresponding Authors

James A. Thomas − *Department of Chemistry, University of Sheffield, Sheffield S3 7HF, U.K.*; orcid.org/0000-0002-8662-7917; Email: james.thomas@sheffield.ac.uk

Sheila MacNeil − *Materials Science & Engineering, University of Sheffield, Sheffield S1 3JD, U.K.*; Email: s.macneil@sheffield.ac.uk

John W. Haycock − *Materials Science & Engineering, University of Sheffield, Sheffield S1 3JD, U.K.*; Email: j.w.haycock@sheffield.ac.uk

Authors

Ahtasham Raza − *Materials Science & Engineering, University of Sheffield, Sheffield S1 3JD, U.K.*

Stuart A. Archer − *Department of Chemistry, University of Sheffield, Sheffield S3 7HF, U.K.*

Simon D. Fairbanks − *Department of Chemistry, University of Sheffield, Sheffield S3 7HF, U.K.*

Kirsty L. Smitten − *Department of Chemistry, University of Sheffield, Sheffield S3 7HF, U.K.*

Stanley W. Botchway − *Central Laser Facility, Research Complex at Harwell, STFC Rutherford Appleton Laboratory, Oxfordshire OX11 0QX, U.K.*

Complete contact information is available at: https://pubs.acs.org/10.1021/jacs.9b11313

Notes

The authors declare no competing financial interest.

■ ACKNOWLEDGMENTS

We are grateful to the EPSRC for postdoctoral funding of S.A.A. and A.R. (EP/M015572/1). We thank our reviewers whose comments have greatly helped in improving the quality of this report.

■ REFERENCES

(1) Daniell, M. D.; Hill, J. S. A History of Photodynamic Therapy. *Aust N Z. J. Surg* **1991**, *61* (5), 340−348.

(2) Moan, J.; Peng, Q. An Outline of the History of PDT. *Photodynamic Therapy*; Royal Society of Chemistry: Cambridge, 2003; pp 1−18.

(3) Allison, R. R.; Mota, H. C.; Sibata, C. H. Clinical PD/PDT in North America: an Historical Review. *Photodiagn. Photodyn. Ther.* **2004**, *1* (4), 263−277.

(4) Dougherty, T. J.; Gomer, C. J.; Henderson, B. W.; Jori, G.; Kessel, D.; Korbelik, M.; Moan, J.; Peng, Q. Photodynamic Therapy. *J. Natl. Cancer Inst.* **1998**, *90* (12), 889−905.

(5) Hsi, R. A.; Rosenthal, D. I.; Glatstein, E. Photodynamic Therapy in the Treatment of Cancer: Current State of the Art. *Drugs* **1999**, *57* (5), 725−734.

(6) Dolmans, D. E. J. G. J.; Fukumura, D.; Jain, R. K. Photodynamic Therapy for Cancer. *Nat. Rev. Cancer* **2003**, *3* (5), 380−387.

(7) Dąbrowski, J. M.; Arnaut, L. G. Photodynamic Therapy (PDT) of Cancer: From Local to Systemic Treatment. *Photochem. Photobiol. Sci.* **2015**, *14* (10), 1765−1780.

(8) Chilakamarthi, U.; Giribabu, L. Photodynamic Therapy: Past, Present and Future. *Chem. Record* **2017**, *17* (8), 775−802.

(9) Castano, A. P.; Demidova, T. N.; Hamblin, M. R. Mechanisms in Photodynamic Therapy: Part One—Photosensitizers, Photochemistry and Cellular Localization. *Photodiagn. Photodyn. Ther.* **2004**, *1* (4), 279−293.

(10) O'Connor, A. E.; Gallagher, W. M.; Byrne, A. T. Porphyrin and Nonporphyrin Photosensitizers in Oncology: Preclinical and Clinical Advances in Photodynamic Therapy. *Photochem. Photobiol.* **2009**, *85* (5), 1053−1074.

(11) Celli, J. P.; Spring, B. Q.; Rizvi, I.; Evans, C. L.; Samkoe, K. S.; Verma, S.; Pogue, B. W.; Hasan, T. Imaging and Photodynamic Therapy: Mechanisms, Monitoring, and Optimization. *Chem. Rev.* **2010**, *110* (5), 2795−2838.

(12) Abrahamse, H.; Hamblin, M. R. New Photosensitizers for Photodynamic Therapy. *Biochem. J.* **2016**, *473* (4), 347−364.

(13) Foote, C. S. Definition of Type I and Type II Photosensitized Oxidation. *Photochem. Photobiol.* **1991**, *54* (5), 659.

(14) Sharman, W. M.; Allen, C. M.; Van Lier, J. E. Photodynamic Therapeutics: Basic Principles and Clinical Applications. *Drug Discovery Today* **1999**, *4* (11), 507−517.

(15) Juarranz, Á.; Jaén, P.; Sanz-Rodríguez, F.; Cuevas, J.; González, S. Photodynamic Therapy of Cancer. Basic Principles and Applications. *Clin. Transl. Oncol.* **2008**, *10* (3), 148−154.

(16) Plaetzer, K.; Krammer, B.; Berlanda, J.; Berr, F.; Kiesslich, T. Photophysics and Photochemistry of Photodynamic Therapy: Fundamental Aspects. *Lasers Med. Sci.* **2009**, *24* (2), 259−268.

(17) Fernandez, J. M.; Bilgin, M. D.; Grossweiner, L. I. Singlet Oxygen Generation by Photodynamic Agents. *J. Photochem. Photobiol., B* **1997**, *37* (1−2), 131−140.

(18) DeRosa, M. C.; Crutchley, R. J. Photosensitized Singlet Oxygen and Its Applications. *Coord. Chem. Rev.* **2002**, *233-234*, 351−371.

(19) Zhou, Z.; Song, J.; Nie, L.; Chen, X. Reactive Oxygen Species Generating Systems Meeting Challenges of Photodynamic Cancer Therapy. *Chem. Soc. Rev.* **2016**, *45* (23), 6597−6626.

(20) Detty, M. R.; Gibson, S. L.; Wagner, S. J. Current Clinical and Preclinical Photosensitizers for Use in Photodynamic Therapy. *J. Med. Chem.* **2004**, *47* (16), 3897−3915.

(21) Kawczyk-Krupka, A.; Bugaj, A. M.; Latos, W.; Zaremba, K.; Sieroń, A. Photodynamic Therapy in Treatment of Cutaneous and Choroidal Melanoma. *Photodiagn. Photodyn. Ther.* **2013**, *10* (4), 503−509.

(22) Ross, K.; Cherpelis, B.; Lien, M.; Fenske, N. Spotlighting the Role of Photodynamic Therapy in Cutaneous Malignancy: an Update and Expansion. *Dermatol. Surg.* **2013**, *39* (12), 1733−1744.

(23) Huang, Z. A. Review of Progress in Clinical Photodynamic Therapy. *Technol. Cancer Res. Treat.* **2005**, *4* (3), 283−293.

(24) Agostinis, P.; Berg, K.; Cengel, K. A.; Foster, T. H.; Girotti, A. W.; Gollnick, S. O.; Hahn, S. M.; Hamblin, M. R.; Juzeniene, A.;

Kessel, D.; et al. Photodynamic Therapy of Cancer: an Update. *Ca-Cancer J. Clin.* **2011**, *61* (4), 250−281.
(25) Baldea, I.; Filip, A. G.; Filip, A. G. 2012. Photodynamic Therapy in Melanoma - an Update. *Journal of Physiology and Pharmacology* **2012**, *63* (2), 109−118.
(26) Nelson, J. S.; McCullough, J. L.; Berns, M. W.; Berns, M. W. Photodynamic Therapy of Human Malignant Melanoma Xenografts in Athymic Nude Mice. *J. Natl. Cancer Inst.* **1988**, *80* (1), 56−60.
(27) Huang, Y.-Y.; Vecchio, D.; Avci, P.; Yin, R.; Garcia-Diaz, M.; Hamblin, M. R. Melanoma Resistance to Photodynamic Therapy: New Insights. *Biol. Chem.* **2013**, *394* (2), 239−250.
(28) Domingues, B.; Lopes, J. M.; Soares, P.; Populo, H. Melanoma Treatment in Review. *ImmunoTargets Ther.* **2018**, *7*, 35−49.
(29) Ergun, E.; Tittl, M.; Stur, M. Photodynamic Therapy with Verteporfin in Subfoveal Choroidal Neovascularization Secondary to Central Serous Chorioretinopathy. *Arch. Ophthalmol.* **2004**, *122* (1), 37−41.
(30) Sheleg, S. V.; Zhavrid, E. A.; Khodina, T. V.; Kochubeev, G. A.; Istomin, Y. P.; Chalov, V. N.; Zhuravkin, I. N. Photodynamic Therapy with Chlorin E_6 For Skin Metastases of Melanoma. *Photodermatol., Photoimmunol. Photomed.* **2004**, *20* (1), 21−26.
(31) Harris, A. L. Hypoxia - a Key Regulatory Factor in Tumour Growth. *Nat. Rev. Cancer* **2002**, *2* (1), 38−47.
(32) Muz, B.; de la Puente; de, P.; Azab, F.; Azab, A. K.; Azab, A. K. The Role of Hypoxia in Cancer Progression, Angiogenesis, Metastasis, and Resistance to Therapy. *Hypoxia* **2015**, *3*, 83−92.
(33) Pawlicki, M.; Collins, H. A.; Denning, R. G.; Anderson, H. L. Two-Photon Absorption and the Design of Two-Photon Dyes. *Angew. Chem., Int. Ed.* **2009**, *48* (18), 3244−3266.
(34) Bolze, F.; Jenni, S.; Sour, A.; Heitz, V. Molecular Photosensitisers for Two-Photon Photodynamic Therapy. *Chem. Commun.* **2017**, *53* (96), 12857−12877.
(35) Mir, Y.; van Lier, J. E.; Allard, J.-F.; Morris, D.; Houde, D. Two-Photon Absorption Cross Section of Excited Phthalocyanines by a Femtosecond Ti-Sapphire Laser. *Photochem. Photobiol. Sci.* **2009**, *8* (3), 391−395.
(36) Xu, C.; Williams, R. M.; Zipfel, W.; Webb, W. W. Multiphoton Excitation Cross-Sections of Molecular Fluorophores. *Bioimaging* **1996**, *4* (3), 198−207.
(37) Karotki, A.; Khurana, M.; Lepock, J. R.; Wilson, B. C. Simultaneous Two-Photon Excitation of Photofrin in Relation to Photodynamic Therapy. *Photochem. Photobiol.* **2006**, *82* (2), 443−452.
(38) Szaciłowski, K.; Macyk, W.; Drzewiecka-Matuszek, A.; Brindell, M.; Stochel, G. Bioinorganic Photochemistry: Frontiers and Mechanisms. *Chem. Rev.* **2005**, *105* (6), 2647−2694.
(39) Allison, R. R.; Sibata, C. H. Oncologic Photodynamic Therapy Photosensitizers: a Clinical Review. *Photodiagn. Photodyn. Ther.* **2010**, *7* (2), 61−75.
(40) Kim, H. M.; Cho, B. R. Small-Molecule Two-Photon Probes for Bioimaging Applications. *Chem. Rev.* **2015**, *115* (11), 5014−5055.
(41) McKenzie, L. K.; Bryant, H. E.; Weinstein, J. A. Transition Metal Complexes as Photosensitisers in One- and Two-Photon Photodynamic Therapy. *Coord. Chem. Rev.* **2019**, *379*, 2−29.
(42) Dhenaut, C.; Ledoux, I.; Samuel, I. D. W.; Zyss, J.; Bourgault, M.; Bozec, H. L. Chiral Metal Complexes with Large Octupolar Optical Nonlinearities. *Nature* **1995**, *374* (6520), 339−342.
(43) Feuvrie, C.; Maury, O.; Le Bozec, H.; Ledoux, I.; Morrall, J. P.; Dalton, G. T.; Samoc, M.; Humphrey, M. G. Nonlinear Optical and Two-Photon Absorption Properties of Octupolar Tris(Bipyridyl)-Metal Complexes. *J. Phys. Chem. A* **2007**, *111* (37), 8980−8985.
(44) Lacroix, P. G.; Malfant, I.; Lepetit, C. Second-Order Nonlinear Optics in Coordination Chemistry: an Open Door Towards Multi-Functional Materials and Molecular Switches. *Coord. Chem. Rev.* **2016**, *308*, 381−394.
(45) Josefsen, L. B.; Boyle, R. W. Photodynamic Therapy and the Development of Metal-Based Photosensitisers. *Met.-Based Drugs* **2008**, *2008* (4), 1−23.
(46) Basu, U.; Khan, I.; Hussain, A.; Kondaiah, P.; Chakravarty, A. R. Photodynamic Effect in Near-IR Light by a Photocytotoxic Iron(III) Cellular Imaging Agent. *Angew. Chem., Int. Ed.* **2012**, *51* (11), 2658−2661.
(47) Higgins, S. L. H.; Brewer, K. J. Designing Red-Light-Activated Multifunctional Agents for the Photodynamic Therapy. *Angew. Chem., Int. Ed.* **2012**, *51* (46), 11420−11422.
(48) Knoll, J. D. Control and Utilization of Ruthenium and Rhodium Metal Complex Excited States for Photoactivated Cancer Therapy. *Coord. Chem. Rev.* **2015**, *282*−*283*, 110−126.
(49) Arenas, Y.; Monro, S.; Shi, G.; Mandel, A.; McFarland, S.; Lilge, L. Photodynamic Inactivation of Staphylococcus Aureus and Methicillin-Resistant Staphylococcus Aureus with Ru(II)-Based Type I/Type II Photosensitizers. *Photodiagn. Photodyn. Ther.* **2013**, *10* (4), 615−625.
(50) Stephenson, M.; Reichardt, C.; Pinto, M.; Wächtler, M.; Sainuddin, T.; Shi, G.; Yin, H.; Monro, S.; Sampson, E.; Dietzek, B.; et al. Ru(II) Dyads Derived From 2-(1-Pyrenyl)-1 H-Imidazo[4,5-F][1,10]Phenanthroline: Versatile Photosensitizers for Photodynamic Applications. *J. Phys. Chem. A* **2014**, *118* (45), 10507−10521.
(51) Frei, A.; Agarwal, C.; Tubafard, S.; Blacque, O.; Anstaett, P.; Felgenträger, A.; Maisch, T.; Spiccia, L.; Gasser, G. Synthesis, Characterization, and Biological Evaluation of New Ru(II) Polypyridyl Photosensitizers for Photodynamic Therapy. *J. Med. Chem.* **2014**, *57* (17), 7280−7292.
(52) Mari, C.; Pierroz, V.; Ferrari, S.; Gasser, G. Combination of Ru(II) Complexes and Light: New Frontiers in Cancer Therapy. *Chem. Sci.* **2015**, *6* (5), 2660−2686.
(53) Liu, J.; Zhang, C.; Rees, T. W.; Ke, L.; Ji, L.; Chao, H. Harnessing Ruthenium(II) as Photodynamic Agents: Encouraging Advances in Cancer Therapy. *Coord. Chem. Rev.* **2018**, *363*, 17−28.
(54) Huang, H.; Yu, B.; Zhang, P.; Huang, J.; Chen, Y.; Gasser, G.; Ji, L.; Chao, H. Highly Charged Ruthenium(II) Polypyridyl Complexes as Lysosome-Localized Photosensitizers for Two-Photon Photodynamic Therapy. *Angew. Chem., Int. Ed.* **2015**, *54*, 14049−14052.
(55) McKenzie, L. K.; Sazanovich, I. V.; Baggaley, E.; Bonneau, M.; Guerchais, V.; Williams, J. A. G.; Weinstein, J. A.; Bryant, H. E. Metal Complexes for Two-Photon Photodynamic Therapy: a Cyclometallated Iridium Complex Induces Two-Photon Photosensitization of Cancer Cells Under Near-IR Light. *Chem. - Eur. J.* **2017**, *23* (2), 234−238.
(56) Tian, X.; Zhu, Y.; Zhang, M.; Luo, L.; Wu, J.; Zhou, H.; Guan, L.; Battaglia, G.; Tian, Y. Localization Matters: a Nuclear Targeting Two-Photon Absorption Iridium Complex in Photodynamic Therapy. *Chem. Commun.* **2017**, *53* (23), 3303−3306.
(57) Heinemann, F.; Karges, J.; Gasser, G. Critical Overview of the Use of Ru(II) Polypyridyl Complexes as Photosensitizers in One-Photon and Two-Photon Photodynamic Therapy. *Acc. Chem. Res.* **2017**, *50* (11), 2727−2736.
(58) Qiu, K.; Wang, J.; Song, C.; Wang, L.; Zhu, H.; Huang, H.; Huang, J.; Wang, H.; Ji, L.; Chao, H. Crossfire for Two-Photon Photodynamic Therapy with Fluorinated Ruthenium (II) Photosensitizers. *ACS Appl. Mater. Interfaces* **2017**, *9* (22), 18482−18492.
(59) Hess, J.; Huang, H.; Kaiser, A.; Kaur, M.; Blacque, O.; Chao, H.; Gasser, G. Evaluation of the Medicinal Potential of Two Ruthenium(II) Polypyridine Complexes as One- and Two-Photon Photodynamic Therapy Photosensitizers. *Chem. - Eur. J.* **2017**, *23* (41), 9888−9896.
(60) Ocana, A.; Pandiella, A.; Siu, L. L.; Tannock, I. F. Preclinical Development of Molecular- Targeted Agents for Cancer. *Nat. Rev. Clin. Oncol.* **2011**, *8* (4), 200−209.
(61) Harrison, R. K. Phase II and Phase III Failures: 2013−2015. *Nat. Rev. Drug Discovery* **2016**, *15* (12), 817−818.
(62) Minchinton, A. I.; Tannock, I. F. Drug Penetration in Solid Tumours. *Nat. Rev. Cancer* **2006**, *6* (8), 583−592.
(63) Imamura, Y.; Mukohara, T.; Shimono, Y.; Funakoshi, Y.; Chayahara, N.; Toyoda, M.; Kiyota, N.; Takao, S.; Kono, S.; Nakatsura, T.; et al. Comparison of 2D- and 3D-Culture Models as

https://dx.doi.org/10.1021/jacs.9b11313
J. Am. Chem. Soc. 2020, 142, 4639−4647

Drug-Testing Platforms in Breast Cancer. *Oncol. Rep.* **2015**, *33* (4), 1837−1843.
(64) Baker, B. M.; Chen, C. S. Deconstructing the Third Dimension-How 3D Culture Microenvironments Alter Cellular Cues. *J. Cell Sci.* **2012**, *125* (13), 3015−3024.
(65) Dubessy, C.; Merlin, J. M.; Marchal, C.; Guillemin, F. Spheroids in Radiobiology and Photodynamic Therapy. *Crit Rev. Oncol Hematol* **2000**, *36* (2−3), 179−192.
(66) Hirschhaeuser, F.; Menne, H.; Dittfeld, C.; West, J.; Mueller-Klieser, W.; Kunz-Schughart, L. A. Multicellular Tumor Spheroids: an Underestimated Tool Is Catching Up Again. *J. Biotechnol.* **2010**, *148* (1), 3−15.
(67) Breslin, S.; O'Driscoll, L. Three-Dimensional Cell Culture: the Missing Link in Drug Discovery. *Drug Discovery Today* **2013**, *18* (5−6), 240−249.
(68) Weiswald, L.-B.; Bellet, D.; Dangles-Marie, V. Spherical Cancer Models in Tumor Biology. *Neoplasia* **2015**, *17* (1), 1−15.
(69) Däster, S.; Amatruda, N.; Calabrese, D.; Ivanek, R.; Turrini, E.; Droeser, R. A.; Zajac, P.; Fimognari, C.; Spagnoli, G. C.; Iezzi, G.; et al. Induction of Hypoxia and Necrosis in Multicellular Tumor Spheroids Is Associated with Resistance to Chemotherapy Treatment. *Oncotarget* **2017**, *8* (1), 1725−1736.
(70) Ramu, V.; Gill, M. R.; Jarman, P. J.; Turton, D.; Thomas, J. A.; Das, A.; Smythe, C. A Cytostatic Ruthenium(II)-Platinum(II) Bis(Terpyridyl) Anticancer Complex That Blocks Entry Into S Phase by Up-Regulating P27 KIP1. *Chem. - Eur. J.* **2015**, *21* (25), 9185−9197.
(71) Gill, M. R.; Derrat, H.; Smythe, C. G. W.; Battaglia, G.; Thomas, J. A. Ruthenium(II) Metallo-Intercalators: DNA Imaging and Cytotoxicity. *ChemBioChem* **2011**, *12* (6), 877−880.
(72) Gill, M. R.; Jarman, P. J.; Halder, S.; Walker, M. G.; Saeed, H. K.; Thomas, J. A.; Smythe, C.; Ramadan, K.; Vallis, K. A. A Three-in-One-Bullet for Oesophageal Cancer: Replication Fork Collapse, Spindle Attachment Failure and Enhanced Radiosensitivity Generated by a Ruthenium(II) Metallo-Intercalator. *Chem. Sci.* **2018**, *9* (4), 841−849.
(73) Jarman, P. J.; Noakes, F.; Fairbanks, S.; Smitten, K.; Griffiths, I. K.; Saeed, H. K.; Thomas, J. A.; Smythe, C. Exploring the Cytotoxicity, Uptake, Cellular Response, and Proteomics of Mono- and Dinuclear DNA Light-Switch Complexes. *J. Am. Chem. Soc.* **2019**, *141* (7), 2925−2937.
(74) Walker, M. G.; Jarman, P. J.; Gill, M. R.; Tian, X.; Ahmad, H.; Reddy, P. A. N.; McKenzie, L.; Weinstein, J. A.; Meijer, A. J. H. M.; Battaglia, G.; et al. A Self-Assembled Metallomacrocycle Singlet Oxygen Sensitizer for Photodynamic Therapy. *Chem. - Eur. J.* **2016**, *22* (17), 5996−6000.
(75) Saeed, H. K.; Archer, S.; Sreedharan, S.; Saeed, I. Q.; Buurma, N. J.; Thomas, J. A. Homo- and Heteroleptic Phototoxic Dinuclear Metallo-Intercalators Based on Ru-II(Dppn) Intercalating Moieties: Synthesis, Optical, and Biological Studies. *Angew. Chem., Int. Ed.* **2017**, *56* (41), 12628−12633.
(76) Archer, S. A.; Raza, A.; Dröge, F.; Robertson, C.; Auty, A. J.; Chekulaev, D.; Weinstein, J. A.; Keane, T.; Meijer, A. J. H. M.; Haycock, J. W.; et al. A Dinuclear Ruthenium(Ii) Phototherapeutic That Targets Duplex and Quadruplex DNA. *Chem. Sci.* **2019**, *10*, 3502−3513.
(77) Elias, B.; Kirsch-DeMesmaeker, A. Photo-Reduction of Polyazaaromatic Ru(II) Complexes by Biomolecules and Possible Applications. *Coord. Chem. Rev.* **2006**, *250* (13−14), 1627−1641.
(78) Ortmans, I. I.; Elias, B. B.; Kelly, J. M. J.; Moucheron, C. C.; Kirsch-DeMesmaeker, A. A. [Ru(TAP)2(Dppz)]2+: a DNA Intercalating Complex, Which Luminesces Strongly in Water and Undergoes Photo-Induced Proton-Coupled Electron Transfer with Guanosine-5′-Monophosphate. *Dalton Trans* **2004**, No. 4, 668−676.
(79) Ghizdavu, L.; Pierard, F.; Rickling, S.; Aury, S.; Surin, M.; Beljonne, D.; Lazzaroni, R.; Murat, P.; Defrancq, E.; Moucheron, C.; et al. Oxidizing Ru(II) Complexes as Irreversible and Specific Photo-Cross-Linking Agents of Oligonucleotide Duplexes. *Inorg. Chem.* **2009**, *48* (23), 10988−10994.
(80) Elias, B.; Creely, C.; Doorley, G. W.; Feeney, M. M.; Moucheron, C.; Kirsch-DeMesmaeker, A.; Dyer, J.; Grills, D. C.; George, M. W.; Matousek, P.; et al. Photooxidation of Guanine by a Ruthenium Dipyridophenazine Complex Intercalated in a Double-Stranded Polynucleotide Monitored Directly by Picosecond Visible and Infrared Transient Absorption Spectroscopy. *Chem. - Eur. J.* **2008**, *14* (1), 369−375.
(81) Hall, J. P.; Poynton, F. E.; Keane, P. M.; Gurung, S. P.; Brazier, J. A.; Cardin, D. J.; Winter, G.; Gunnlaugsson, T.; Sazanovich, I. V.; Towrie, M.; et al. Monitoring One-Electron Photo-Oxidation of Guanine in DNA Crystals Using Ultrafast Infrared Spectroscopy. *Nat. Chem.* **2015**, *7* (12), 961−967.
(82) Cardin, C. J.; Kelly, J. M.; Quinn, S. J. Photochemically Active DNA-Intercalating Ruthenium and Related Complexes − Insights by Combining Crystallography and Transient Spectroscopy. *Chem. Sci.* **2017**, *8* (7), 4705−4723.
(83) Baggaley, E.; Gill, M. R.; Green, N. H.; Turton, D.; Sazanovich, I. V.; Botchway, S. W.; Smythe, C.; Haycock, J. W.; Weinstein, J. A.; Thomas, J. A. Dinuclear Ruthenium(II) Complexes as Two-Photon, Time-Resolved Emission Microscopy Probes for Cellular DNA. *Angew. Chem., Int. Ed.* **2014**, *53* (13), 3367−3371.
(84) Kessel, D.; Luo, Y. Mitochondrial Photodamage and PDT-Induced Apoptosis. *J. Photochem. Photobiol., B* **1998**, *42* (2), 89−95.
(85) Morgan, J.; Oseroff, A. R. Mitochondria-Based Photodynamic Anti-Cancer Therapy. *Adv. Drug Delivery Rev.* **2001**, *49* (1−2), 71−86.
(86) Makarov, N. S.; Drobizhev, M.; Rebane, A. Two-Photon Absorption Standards in the 550−1600 Nm Excitation Wavelength Range. *Opt. Express* **2008**, *16* (6), 4029−4047.
(87) Ogawa, K.; Kobuke, Y. Two-Photon Photodynamic Therapy by Water-Soluble Self-Assembled Conjugated Porphyrins. *BioMed Res. Int.* **2013**, *2013* (11), 1−11.
(88) Khurana, M.; Collins, H. A.; Karotki, A.; Anderson, H. L.; Cramb, D. T.; Wilson, B. C. Quantitative in Vitro Demonstration of Two-Photon Photodynamic Therapy Using Photofrin ®and Visudyne ®. *Photochem. Photobiol.* **2007**, *83* (6), 1441−1448.
(89) Raza, A.; Colley, H. E.; Baggaley, E.; Sazanovich, I. V.; Green, N. H.; Weinstein, J. A.; Botchway, S. W.; MacNeil, S.; Haycock, J. W. Oxygen Mapping of Melanoma Spheroids Using Small Molecule Platinum Probe and Phosphorescence Lifetime Imaging Microscopy. *Sci. Rep.* **2017**, *7* (1), 10743.
(90) Sitnik, T. M.; Henderson, B. W. The Effect of Fluence Rate on Tumor and Normal Tissue Responses to Photodynamic Therapy. *Photochem. Photobiol.* **1998**, *67* (4), 462−466.
(91) Henderson, B. W.; Busch, T. M.; Vaughan, L. A.; Frawley, N. P.; Babich, D.; Sosa, T. A.; Zollo, J. D.; Dee, A. S.; Cooper, M. T.; Bellnier, D. A.; et al. Photofrin Photodynamic Therapy Can Significantly Deplete or Preserve Oxygenation in Human Basal Cell Carcinomas During Treatment, Depending on Fluence Rate. *Cancer Res.* **2000**, *60* (3), 525−529.
(92) Dysart, J. S.; Patterson, M. S. Characterization of Photofrin Photobleaching for Singlet Oxygen Dose Estimation During Photodynamic Therapy of MLL Cells in Vitro. *Phys. Med. Biol.* **2005**, *50* (11), 2597−2616.
(93) Seshadri, M.; Bellnier, D. A.; Vaughan, L. A.; Spernyak, J. A.; Mazurchuk, R.; Foster, T. H.; Henderson, B. W. Light Delivery Over Extended Time Periods Enhances the Effectiveness of Photodynamic Therapy. *Clin. Cancer Res.* **2008**, *14* (9), 2796−2805.
(94) Gallagher Colombo, S. M.; Finlay, J. C.; Busch, T. M. Tumor Microenvironment as a Determinant of Photodynamic Therapy Resistance. In *Resistance to Photodynamic Therapy in Cancer*; Resistance to Targeted Anti-Cancer Therapeutics; Springer International Publishing: Cham, 2014; Vol. *5*, pp 65−97.
(95) Ortonne, J.-P. Photoprotective Properties of Skin Melanin. *Br. J. Dermatol.* **2002**, *146* (61), 7−10.
(96) Vera, R. E.; Lamberti, M. J.; Rivarola, V. A.; Rumie Vittar, N. B. Developing Strategies to Predict Photodynamic Therapy Outcome: the Role of Melanoma Microenvironment. *Tumor Biol.* **2015**, *36* (12), 9127−9136.

https://dx.doi.org/10.1021/jacs.9b11313
J. Am. Chem. Soc. 2020, 142, 4639−4647

(97) Sharma, K. V.; Bowers, N.; Davids, L. M. Photodynamic Therapy-Induced Killing Is Enhanced in Depigmented Metastatic Melanoma Cells. *Cell Biol. Int.* **2011**, *35* (9), 939−944.

https://dx.doi.org/10.1021/jacs.9b11313
J. Am. Chem. Soc. 2020, 142, 4639−4647